Non-Gaussian structure of the lensed CMB power spectra covariance matrix

Aurélien Benoit-Lévy,[1,*] Kendrick M. Smith,[2] and Wayne Hu[3]

[1]*UPMC-CNRS, UMR7095, Institut d'Astrophysique de Paris, 75014 Paris, France*
[2]*Department of Astrophysical Sciences, Princeton University, Princeton, New Jersey 08544-1001, USA*
[3]*Department of Astronomy and Astrophysics, Kavli Institute for Cosmological Physics, University of Chicago, Chicago, Illinois 60637, USA*

Gravitational lensing of the cosmic microwave background (CMB) encodes cosmological information in the observed anisotropies of temperature and polarization. Accurate extraction of this additional information requires precise modeling of the covariance matrix of the power spectra of observed CMB fields. We introduce a new analytical model to describe the non-Gaussian structure of this covariance matrix and display the importance of second-order terms that were previously neglected. When compared with direct numerical simulations our model captures parameter errors to better than a few percent for cases where the non-Gaussianity causes an order unity degradation in errors. We also provide a detailed comparison between the information content of lensed CMB power spectra and ideal reconstruction of the lensing potential. We illustrate the impact of the non-Gaussian terms in the power spectrum covariance by providing Fisher errors on the sum of the masses of the neutrinos, the dark energy equation of state, and the curvature of the Universe.

I. INTRODUCTION

Gravitational potentials of large-scale structure generate a deflection of the trajectories of the cosmic microwave background (CMB) photons, an effect known as CMB lensing [1–3] (see Ref. [4] for a review). After its initial detection in cross correlation with large-scale structure [5,6], CMB lensing has now been detected with high significance in high-resolution observations from the Atacama Cosmology Telescope [7,8] and the South Pole Telescope [9].

CMB lensing generates a characteristic statistical signature that makes the CMB sensitive to cosmological parameters which directly influence the growth of cosmic structure. This breaks the angular diameter degeneracy in the unlensed CMB and improves constraints on parameters such as neutrino masses, the dark energy equation of state, and the curvature of the Universe [10–14].

Mathematically, CMB lensing is described as follows. We introduce a vector field $\mathbf{d}(\hat{\mathbf{n}})$ (the deflection field) such that the lensed temperature $T(\hat{\mathbf{n}})$ and unlensed temperature $\tilde{T}(\hat{\mathbf{n}})$ are related by

$$T(\hat{\mathbf{n}}) = \tilde{T}(\hat{\mathbf{n}} + \mathbf{d}(\hat{\mathbf{n}})) \qquad (1)$$

and analogously for the Stokes parameters $Q(\hat{\mathbf{n}})$, $U(\hat{\mathbf{n}})$ which describe linear CMB polarization. To lowest order in perturbation theory, the deflection field $\mathbf{d}(\hat{\mathbf{n}})$ is the gradient of a scalar lensing potential [i.e., $\mathbf{d}(\hat{\mathbf{n}}) = \nabla\phi(\hat{\mathbf{n}})$] which can be written as a line-of-sight integral:

$$\phi(\hat{\mathbf{n}}) = -2 \int d\eta \, \frac{\chi(\eta - \eta_{\mathrm{rec}})}{\chi(\eta_{\mathrm{rec}})\chi(\eta)} \Psi(\chi\hat{\mathbf{n}}, \eta), \qquad (2)$$

where Ψ is the Newtonian potential, η is conformal time, η_{rec} is the epoch of last scattering, and χ is the angular diameter distance in comoving coordinates.

CMB lensing modifies the Gaussian statistics of the unlensed CMB by generating a correlation between the primary field and its gradient [15]. It also modifies the shape of the temperature and E-mode polarization power spectra, and generates a nonzero B-mode power spectrum. This leads to two different statistical techniques for extracting cosmological information from CMB lensing. First, we can simply make precise measurements of CMB power spectra (especially the B-mode power spectrum), which will include lensing contributions. Second, we can reconstruct the lensing potential ϕ using correlations between the primary field and its gradient, providing a new cosmological observable [16–20].

Accurate analysis of CMB anisotropies requires correct modeling of the covariance matrix of the lensed power spectra. The lensed CMB is not a Gaussian field, and so its power spectrum covariance is nontrivial; in particular the off-diagonal correlations are important. Calculations of the non-Gaussian covariance of the lensed power spectra have been performed in both flat sky [21,22] and full-sky [23] cases, but these calculations make the approximation that some high-order terms in the lensing potential are negligible.

In the advent of low-noise and high-resolution CMB experiments that will be able to probe polarization of the CMB at the arcminute scale (SPTPol, ACTPol [24], POLARBEAR [25]), it becomes necessary to assess the validity of the current approximations for the non-Gaussian power spectrum covariance, and study the impact on cosmological parameter estimation. The purpose of this paper is therefore to investigate in detail the impact of the

*benoitl@iap.fr

non-Gaussianities induced by CMB lensing and quantify the information contained in the power spectra. We introduce a new semianalytical approach to compute the power spectrum covariance matrix and validate our model by Monte Carlo simulations.

In Sec. II, we describe the simulations we performed to estimate the power spectrum covariance matrix and present our semianalytical model. In Sec. III, we introduce a model-independent way of characterizing the relative information content of lensed power spectra and idealized direct reconstruction. Finally, in Sec. IV, we apply this characterization to specific cosmological model parameters.

Throughout the paper, we use a fiducial flat ΛCDM model with the following parameters:

$$\left\{\Omega_c h^2, \Omega_b h^2, h, \tau, n_s, 10^9 A_s, \sum m_\nu\right\}$$

$$= \{0.1096, 0.0226, 0.693, 0.089, 0.964, 2.419, 0.58 \text{ eV}\}. \tag{3}$$

We chose a large fiducial value of m_ν so as to be testable with CMB lensing in the near future.

II. NON-GAUSSIAN POWER SPECTRUM COVARIANCE

To characterize the information content in CMB power spectra we first require an accurate characterization of the covariance matrix between the band power estimates of the temperature and polarization fields. Previous analytic characterizations have been based on a perturbative expansion of the effect of lensing [21,23] which breaks down in the damping tail. In this section, we first conduct a suite of simulations to characterize the covariance and then develop analytic tools which characterize its main features.

A. Simulations

We simulate the lensed CMB on the full sky using the following procedure. We first make a realization of the unlensed CMB fields $\tilde{T}$, $\tilde{E}$ and lensing potential ϕ in harmonic space, treating these fields as Gaussian and computing power spectra using the publicly available Boltzmann code CAMB [26] to $\ell_{\max} = 5000$. Using a fast spherical harmonic transform, we compute the unlensed temperature and polarization in pixel space, using an equicylindrical pixelization with $(N_\theta, N_\phi) = (16384, 32768)$ equally spaced points in (θ, ϕ). We then evaluate the lensed temperature and polarization fields

$$X(\hat{\mathbf{n}}) = \tilde{X}(\hat{\mathbf{n}} + \mathbf{d}(\hat{\mathbf{n}})), \tag{4}$$

where $X \in \{T, Q, U\}$ and tildes distinguish unlensed from lensed fields throughout, at each point of an $N_{\text{side}} = 4096$ Healpix pixelization [27], using cubic interpolation on the equicylindrical map to evaluate the right-hand side, and parallel translation of the spin-2 field $Q \pm iU$ to transport polarization at the point $(\hat{\mathbf{n}} + \mathbf{d}(\hat{\mathbf{n}}))$ to the point $\hat{\mathbf{n}}$. (We use an equicylindrical pixelization for the unlensed fields,

rather than an irregular pixelization such as Healpix, so that interpolation is straightforward to implement). Taking another spherical transform to obtain lensed T, E, and B maps in harmonic space, we compute lensed power spectra $\hat{C}_\ell^{XY}$ for $XY \in \{TT, TE, EE, BB\}$. As a memory optimization, we avoid storing full-sky maps by ''striping'' the sky into 16 latitude bands, and calculate the contribution to $a_{\ell m}^T$, $a_{\ell m}^E$, $a_{\ell m}^B$ from each band before moving onto the next. This allows each simulation to fit onto a single core with ~ 2 GB memory. The above procedure is similar algorithmically to the publicly available code LensPix [28], although the two codes differ in minor details of implementation.

We first compare the mean over the $N = 32768$ realizations

$$\bar{C}_\ell^{XY} = \frac{1}{N} \sum_{\alpha=1}^N \hat{C}_{\ell,\alpha}^{XY}, \tag{5}$$

where $XY \in TT$, TE, EE, BB to the predicted lensed power spectra computed by CAMB. With the resolution parameters given above, the lensed CMB power spectra of the simulations agree with CAMB's calculation of the lensed C_ℓ^{XY}'s to better than 0.1% for all spectra at $\ell_{\max} = 3000$.

We then estimate the covariance matrix between two different power spectra XY and ZW as

$$\text{Cov}_{\ell_1 \ell_2}^{XY, ZW} = \frac{1}{N} \sum_{\alpha=1}^N \hat{C}_{\ell_1, \alpha}^{XY} \hat{C}_{\ell_2, \alpha}^{ZW} - \bar{C}_{\ell_1}^{XY} \bar{C}_{\ell_2}^{ZW}. \tag{6}$$

Even in these noise-free simulations, the Gaussian random variance from the unlensed CMB makes the estimate of the covariance between individual multipoles noisy. We therefore further bin the power spectrum estimators into band powers

$$D_i^{XY} = \sum_\ell B_i^\ell C_\ell^{XY}, \tag{7}$$

where B_i^ℓ is a top hat function

$$B_i^\ell = \begin{cases} \frac{1}{\ell_{i+1} - \ell_i}, & \ell_i \le \ell < \ell_{i+1} \\ 0, & \text{otherwise} \end{cases}. \tag{8}$$

The band width is chosen to be sufficiently small so as to resolve the acoustic features in the spectrum. In practice we take every multipole to $\ell = 25$ followed by uniform bands of $\ell_{i+1} - \ell_i = 15$. We choose not to bin the 25 first multipoles as the derivatives of the power spectrum with respect to cosmological parameters exhibit strong variation at low multipoles, and averaging these variations to one single bin at low ℓ would give erroneous final results. The covariance matrix between these band estimators then becomes

$$\text{Cov}_{ij}^{XY, ZW} = \sum_{\ell_1, \ell_2} B_i^{\ell_1} \text{Cov}_{\ell_1 \ell_2}^{XY, ZW} B_j^{\ell_2}. \tag{9}$$

The Monte Carlo band power covariance is shown in Fig. 1. For visualization purposes, it is convenient to scale out the diagonal contributions by defining the correlation matrix
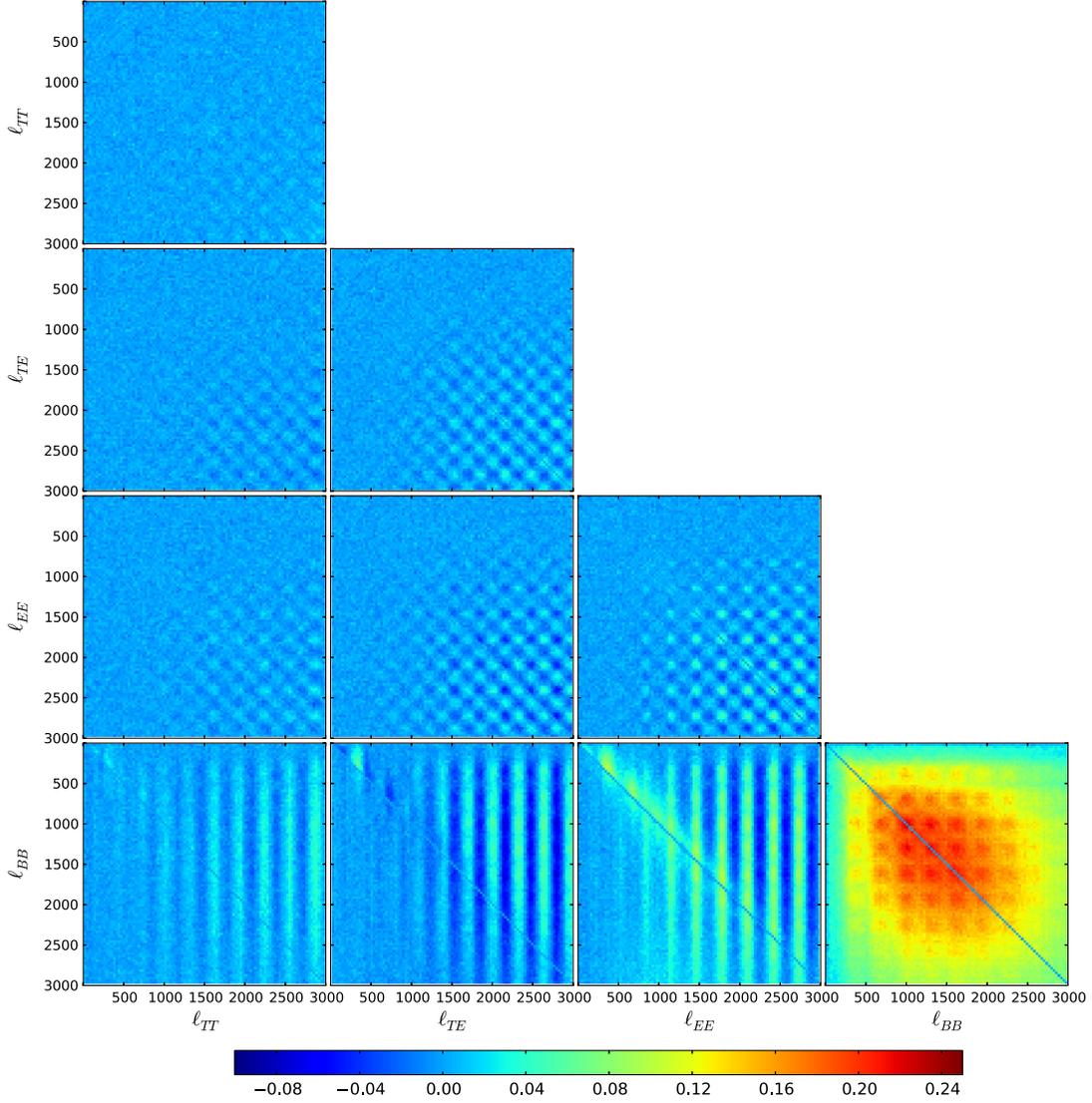
FIG. 1 (color online).   Monte Carlo covariance of the lensed CMB band powers computed from 32768 lensed CMB simulations in bands of $\Delta\ell = 30$. From left to right and top to bottom: TT, TE, EE, and BB. For visualization purposes we plot the correlation coefficient R defined in Eq. (10). The diagonal (of order unity) has been subtracted to enhance contrast.

$$R_{ij}^{XY,ZW} = \frac{\mathrm{Cov}_{ij}^{XY,ZW}}{\sqrt{\mathrm{Cov}_{ii}^{XY,XY}\mathrm{Cov}_{jj}^{ZW,ZW}}}. \qquad (10)$$

For display purposes, we also use a flat binning scheme by dividing the range of multipoles [2–3000] in 100 bins in Figs. 1–5. As expected from previous studies, the covariance of the B modes is highly non-Gaussian [21,23,29]. Interestingly, the EE, BB and EE, EE correlations in Fig. 1 are substantially larger than expected from the lowest-order analytic calculations in Refs. [21,23], and all but TT, TT show clear evidence for correlated structure on the acoustic scale that is again not expected. Although Ref. [21] also conducted simulation tests, their bands were much wider than the acoustic scale such that these structures were hidden.

B. Analytic approximation

In order to develop a new analytic approximation to the covariance matrix, it is useful to first examine the BB, BB correlation for which the existing models work well. The dominant terms in the analytic BB, BB correlation expression can be compactly written as [cf. Ref. [29] Eq. (17)]

$$\mathrm{Cov}_{\ell_1\ell_2}^{BB,BB} = \frac{2}{2\ell_1+1}(C_{\ell_1}^{BB})^2\delta_{\ell_1,\ell_2}$$

$$+ \sum_\ell \left(\frac{\partial C_{\ell_1}^{BB}}{\partial C_\ell^{\tilde{E}\tilde{E}}} \mathrm{Cov}_{\ell\ell}^{\tilde{E}\tilde{E},\tilde{E}\tilde{E}} \frac{\partial C_{\ell_2}^{BB}}{\partial C_\ell^{\tilde{E}\tilde{E}}}\right)$$

$$+ \sum_\ell \left(\frac{\partial C_{\ell_1}^{BB}}{\partial C_\ell^{\phi\phi}} \mathrm{Cov}_{\ell\ell}^{\phi\phi,\phi\phi} \frac{\partial C_{\ell_2}^{BB}}{\partial C_\ell^{\phi\phi}}\right), \qquad (11)$$
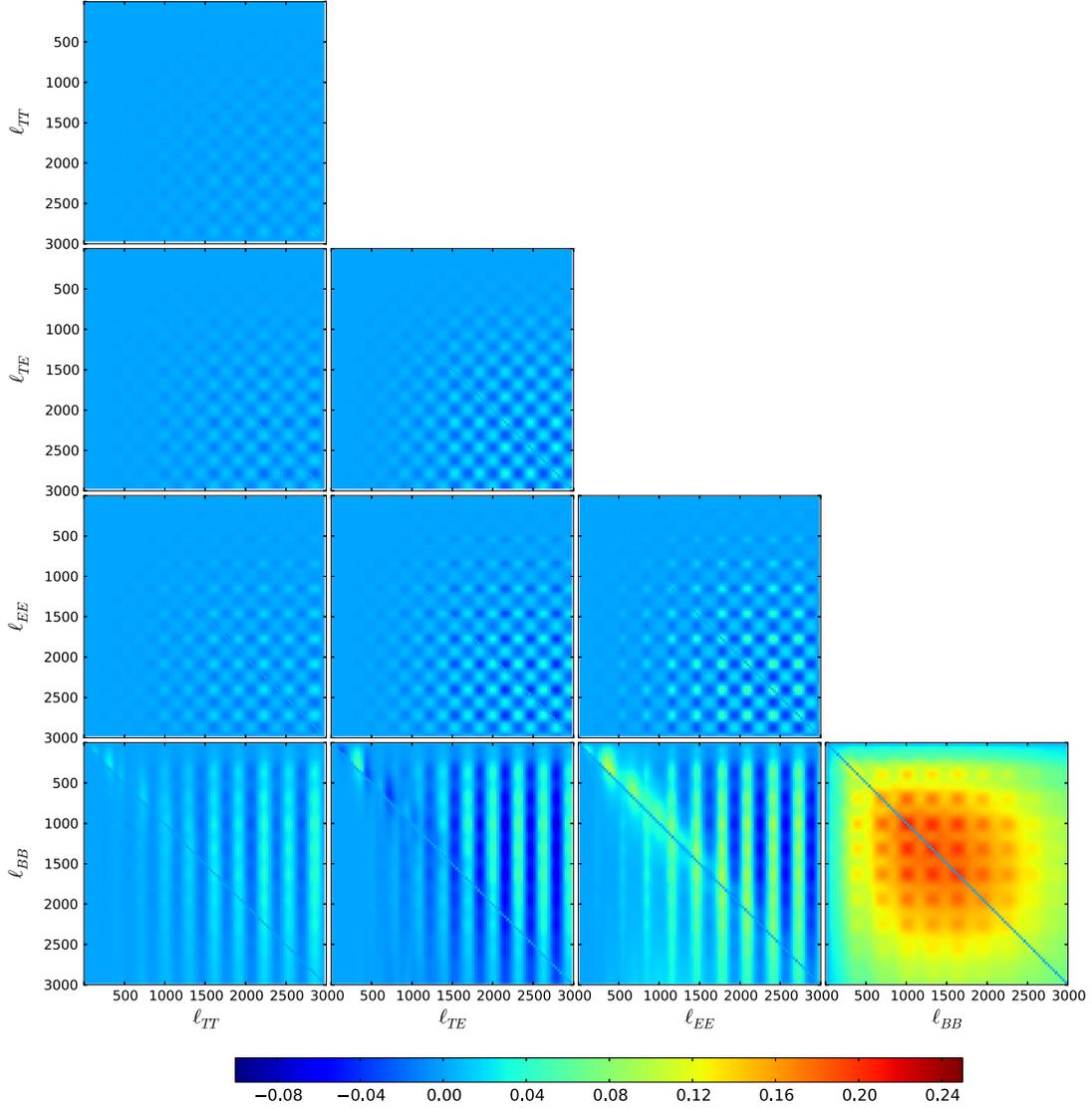
FIG. 2 (color online). Covariance of the lensed CMB band powers in bands of $\Delta \ell = 30$, computed using the analytic model from Sec. II B. From left to right and top to bottom: *TT*, *TE*, *EE*, and *BB*. For visualization purposes we plot the correlation coefficient *R* defined in Eq. (10). Detailed comparison with the Monte Carlo covariance from Fig. 1 shows that the agreement is excellent.

where unlensed CMB power spectra are denoted with tildes and $C_\ell^{\phi\phi}$ is the lensing potential power spectrum. Assuming that these fields are Gaussian, we can use the general prescription for Gaussian random fields G,

$$\text{Cov}_{\ell\ell'}^{G_a G_b, G_c G_d} = \frac{\delta_{\ell,\ell'}}{2\ell+1}[C_\ell^{G_a G_c} C_\ell^{G_b G_d} + C_\ell^{G_a G_d} C_\ell^{G_b G_c}], \quad (12)$$

for the unlensed CMB and ϕ fields.

To calculate power spectrum derivatives such as the ones appearing in Eq. (11), we take finite differences between lensed CMB power spectra computed using CAMB, rather than using a perturbative expansion in deflection angles. Since CAMB's algorithm for computing lensed CMB power spectra includes terms of high order in deflection

angles [30], this approach to computing derivatives also includes high-order terms, and in particular does not break down at high ℓ. Some implementational details of the derivative calculation are presented in the Appendix. The model of Eq. (11) for the correlation matrix is shown in Fig. 2.

Let us try to interpret the terms in Eq. (11). The first term is the usual unconnected piece of the covariance that is the only term for a Gaussian random field. We will loosely refer to this term as the "Gaussian piece". The second and third terms involve the fact that the B field is constructed out of an unlensed $\tilde{E}$ field and the lens potential field ϕ. In the second term, two *BB* band powers are connected by the covariance of the unlensed $\tilde{E}$ fields they share. In the third term, they are connected by the shared ϕ fields. Contributions to the correlation matrix for the second and third terms are shown separately in Fig. 3.
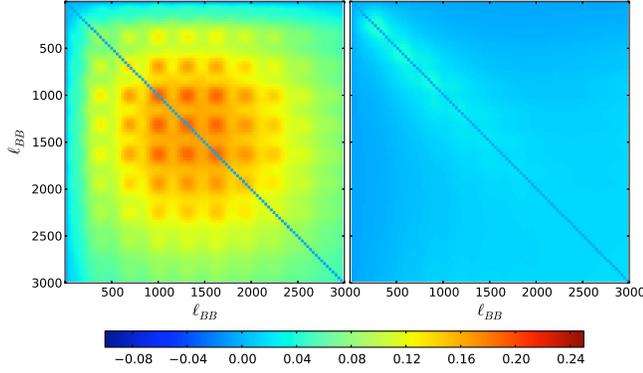
FIG. 3 (color online). Contributions of the individual terms in Eq. (11) to the correlation matrix between *BB* band powers. Left: cosmic variance of the lens power [third term in Eq. (11)]. Right: cosmic variance of the unlensed $\tilde{E}\tilde{E}$ spectrum (second term).

The second term can therefore be interpreted as the covariance in *BB* band powers generated by cosmic variance of the unlensed $\tilde{E}\tilde{E}$ power spectrum. The covariance it generates is positive definite in that enhanced power in $\tilde{E}\tilde{E}$ leads to enhanced *BB* across the spectrum thus correlating modes (see Fig. 3, right panel).

The third term is the cosmic variance of the lens power. Here the correlation reflects the acoustic structure of the unlensed $\tilde{E}\tilde{E}$ power spectrum. More power in the lenses allows more power from the acoustic peaks to transfer into *B* modes than the acoustic troughs (see Fig. 3, left panel).

Finally, we note that Eq. (11) omits a fully connected term where the $\tilde{E}$ and ϕ fields are cross connected involving four unique multipoles rather than three. These contributions tend to sum incoherently and are subdominant in the covariance [23]. We omit this term in our analytic model.
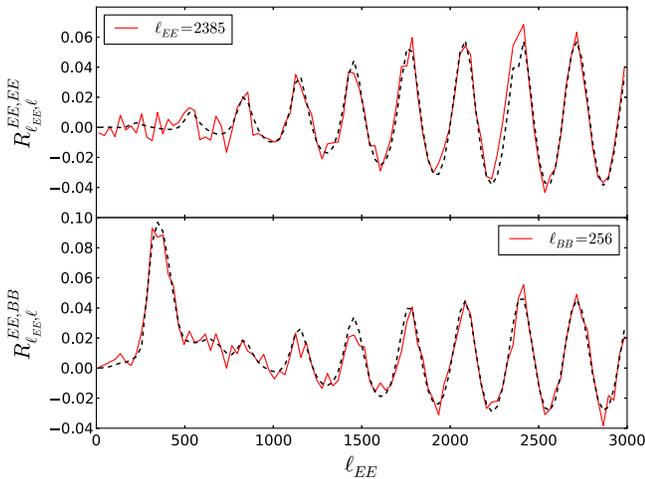
FIG. 4 (color online). Rows of the correlation matrix R, defined in Eq. (10), between *EE-EE* band powers (top), and *EE-BB* (bottom), computed using either Monte Carlo simulations (solid lines) or our analytic model (dashed lines). Binning scheme follows Fig. 1 and the autocorrelation is omitted.
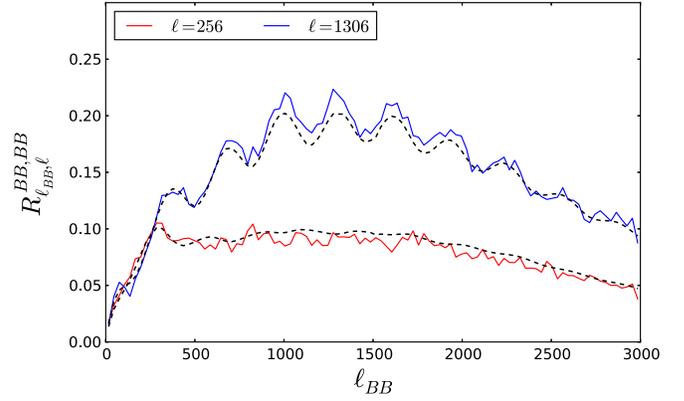
FIG. 5 (color online). Rows of the correlation matrix R, as in Fig. 4, between *BB-BB* band powers computed using either Monte Carlo simulations (solid lines) or our analytic model (dashed lines). Binning scheme follows Fig. 1 and the autocorrelation is omitted. The upper curves are for $\ell = 1306$.

We can use these results to model the other covariance terms. First consider *BB*, *XY* where $XY \in TT, EE, TE$. In this case, there are no Gaussian or unconnected terms and

$$\text{Cov}_{\ell_1\ell_2}^{BB,XY} = \sum_\ell \left(\frac{\partial C_{\ell_1}^{BB}}{\partial C_\ell^{\tilde{E}\tilde{E}}} \text{Cov}_{\ell\ell}^{\tilde{E}\tilde{E},\tilde{X}\tilde{Y}} \frac{\partial C_{\ell_2}^{XY}}{\partial C_\ell^{\tilde{X}\tilde{Y}}} \right)$$
$$+ \sum_\ell \left(\frac{\partial C_{\ell_1}^{BB}}{\partial C_\ell^{\phi\phi}} \text{Cov}_{\ell\ell}^{\phi\phi,\phi\phi} \frac{\partial C_{\ell_2}^{XY}}{\partial C_\ell^{\phi\phi}} \right). \quad (13)$$

In the perturbative limit for the deflection angles, this expression exactly models all terms in the covariance. However, again our expression has extended validity since the derivatives are evaluated nonlinearly with CAMB.

The case of $XY = EE$ is illustrative as there is a substantial correlation. The cosmic variance of the unlensed $\tilde{E}\tilde{E}$ power spectrum produces contributions along the diagonal but biased to a lower *BB* multipole $\ell_1 < \ell_2$. This is due to the fact that most of the power in the low multipoles of *BB* actually comes from where the unlensed $\tilde{E}\tilde{E}$ spectrum peaks ($\ell_1 \sim 1000$). In previous analytic approaches, the term that was kept was for $\ell_2 = \ell$, which is linear in $C_\ell^{\phi\phi}$.

Previous approaches have dropped the term associated with the cosmic variance of the lens power spectrum [the second term in Eq. (13)] under the justification that it is second order in $C_\ell^{\phi\phi}$. In fact it is the dominant contribution to the covariance at $\ell_1, \ell_2 \gtrsim 10^3$. This term causes a band structure in the *EE* dependence of the covariance. Increasing the power in the lenses causes more power from acoustic peaks in $\tilde{E}\tilde{E}$ to be transformed into *BB* power while also filling in power in *EE* at the acoustic troughs. Thus peaks in *EE* are anticorrelated with *BB* and troughs are correlated.

Finally, there are the cases for which $XY, WZ \in TT, TE, EE$. These cases are in principle more complicated in that even at the perturbative level there are many terms that are

not associated with the cosmic variance of unlensed and lens potential power spectra. These are terms that connect the various unlensed, lensed, and lens potential multipoles in the 4 point function. As in the case of BB, BB we can again use the perturbative approximation as a guide. Here, there is a cancellation between the power spectrum covariance terms and the other terms associated with the unlensed fields for slowly varying unlensed power spectra. These other terms reflect the fact that at high CMB multipole moment, the unlensed fields are all lensed by the same large-scale lens realization. For a fixed lens, neighboring bands are anticorrelated by the exchange of power between them. This effect does not occur for the covariances with BB since there is no unlensed B field from which power can be taken.

Given this close cancellation between terms associated with the unlensed fields, we model only the cosmic variance of the lens power spectra in these cases. For XY, $WZ \in TT$, TE, EE,

$$
\begin{aligned}
\text{Cov}_{\ell_1\ell_2}^{XY,WZ} = &\frac{1}{2\ell_1+1}[C_{\ell_1}^{XW}C_{\ell_1}^{YZ} + C_{\ell_1}^{XZ}C_{\ell_1}^{YW}]\delta_{\ell_1,\ell_2} \\
&+ \sum_{\ell}\left[\frac{\partial C_{\ell_1}^{XY}}{\partial C_{\ell}^{\phi\phi}}\,\text{Cov}_{\ell\ell}^{\phi\phi,\phi\phi}\,\frac{\partial C_{\ell_2}^{WZ}}{\partial C_{\ell}^{\phi\phi}}\right].
\end{aligned} \quad (14)
$$

In these cases the covariance takes a checkerboard pattern. For TT, TT or EE, EE enhanced lensing power makes modes near acoustic peaks smaller and larger near troughs. Thus peaks are correlated with peaks, troughs with troughs, and peaks are anticorrelated with troughs.

Combining Eqs. (11), (13), and (14), we have now developed an analytic model for the lensed CMB band power covariance in all cases. Comparison with the Monte Carlo covariance from Sec. II A shows that the difference is typically $\lesssim 10\%$, leading to discrepancies in parameter uncertainties on the order of 5% or less. We will explore this in more detail in Sec. IV C.

III. MODEL-INDEPENDENT LENSING INFORMATION

As mentioned in the introduction, cosmological information from CMB lensing can be obtained either from precise measurements of lensed CMB power spectra or by applying lens reconstruction techniques. In this section, we will quantify the relative amount of cosmological information which can be obtained using these two methods, in a model-independent way which uses Fisher information matrix techniques.

In Sec. III A, we review the Fisher matrix formalism as applied to the lensing potential power spectrum. In Sec. III B we construct the Karhunen-Loève (KL) basis to consider the relative information content. In Sec. III C, we illustrate the necessity to take into account the non-Gaussian terms computed in Sec. II. Finally in Sec. III D, we apply our formalism to realistic CMB experiments.

A. Fisher information

The Fisher information matrix quantifies the information in a given data set whose covariance matrix is known on a set of parameters p_α of interest. In order to quantify the lensing information in a model-independent manner, instead of taking cosmological parameters we take the power spectrum $C_\ell^{\phi\phi}$ itself as the parameters of interest. The effect of any cosmological parameter of present or future interest can be thought of as a specific sum of these parameters. Rather than taking every ℓ as a parameter, we follow Ref. [21] and implicitly assume that the power spectrum is smooth in ℓ so that we can approximate it with binned perturbations around the fiducial model. For each bin α in $C_\ell^{\phi\phi}$, we define a parameter p_α by

$$
\ln C_\ell^{\phi\phi} = \ln C_\ell^{\phi\phi}|_{\text{fid}} + \sum_{\alpha=1}^{N_\phi} p_\alpha B_\alpha^{\phi,\ell}, \quad 0 \le \ell \le \ell_{\text{max}}^\phi, \quad (15)
$$

where $B_\alpha^{\phi,\ell}$ describes the banding and is defined as

$$
B_\alpha^{\phi,\ell} = \begin{cases} 1, & \ell_\alpha < \ell < \ell_{\alpha+1} \le \ell_{\text{max}}^\phi \\ 0, & \text{otherwise} \end{cases}. \quad (16)
$$

In practice, we choose ϕ bands with width $\Delta\ell = 20$ (i.e., $N_\phi = 40$ for $\ell_{\text{max}}^\phi = 2000$ and $N_\phi = 60$ for $\ell_{\text{max}}^\phi = 3000$). We define bands in $\ln C_\ell^{\phi\phi}$ so that the power spectrum remains positive definite for large deviations.

Note that any cosmological parameter variation that predicts a sufficiently smooth deviation from the fiducial model of $\delta \ln C_\ell^{\phi\phi}$ can be represented in these parameters as

$$
p_\alpha = \frac{1}{(\Delta\ell)_\alpha} \sum_\ell \delta \ln C_\ell^{\phi\phi} B_\alpha^{\phi,\ell}, \quad (17)
$$

where $(\Delta\ell)_\alpha$ is the width of bin α.

In general, given some data vector D_I which depends on parameters p_α, the Fisher matrix is given by

$$
F_{\alpha\beta} = \sum_{IJ}\left(\frac{\partial D_I}{\partial p_\alpha}\right)(\text{Cov}_{IJ}^{D,D})^{-1}\left(\frac{\partial D_J}{\partial p_\beta}\right). \quad (18)
$$

We define a Fisher matrix $F_{\alpha\beta}^P$ by specializing to the case where the parameters p_α are the ϕ band powers defined in Eq. (17) and the data vector D_I is the set of lensed CMB band powers D_i^{XY} (where $XY \in TT$, TE, EE, BB) defined in Eq. (7). The derivatives $(\partial D_I/\partial p_\alpha)$ appearing in the Fisher matrix are computed nonlinearly using CAMB, as described in the previous section.

Unless otherwise stated, our model for the covariance matrix $\text{Cov}_{IJ}^{D,D}$ will be based on the semianalytical model from Sec. II B. (We show below that using the Monte Carlo covariance matrix from Sec. II A gives essentially identical parameter uncertainties). We modify this all sky, cosmic variance limited covariance in two ways. First we include the possibility that the measurements contain Gaussian noise terms by replacing the Gaussian diagonal elements with

$$\text{Cov}_{\ell\ell}^{XY,X'Y'} = \frac{1}{2\ell+1}[(C_\ell^{XX'} + N_\ell^{XX'})(C_\ell^{YY'} + N_\ell^{YY'})$$
$$+ (C_\ell^{XY'} + N_\ell^{XY'})(C_\ell^{YX'} + N_\ell^{YX'})], \quad (19)$$

where $N_\ell^{XX'}$ is the noise (cross) power spectrum. Second, we rescale the whole resulting matrix by $1/f_{\text{sky}}$ where f_{sky} is the fraction of sky covered by the data set under the usual assumption that the survey is sufficiently large that correlations across $\Delta\ell \sim 2\pi/\theta_{\text{survey}}$ induced by the fundamental mode of the survey or sky cuts are irrelevant across the acoustic separation. Also we are mainly interested in the effects of the non-Gaussian terms in the CMB covariance matrix at high ℓ. An accurate forecast of parameter constraints or an analysis on data would require a more detailed modeling of the shape of the survey (e.g., by introducing a minimum multipole ℓ_{min}).

The Fisher matrix $F_{\alpha\beta}^P$ defined in this way quantifies the lensing information (in the form of constraints on the ϕ band powers p_α) which can be obtained from noisy measurements of the lensed CMB power spectrum.

We seek to compare this Fisher matrix to

$$F_{\alpha\beta}^R = \sum_{\ell\ell'} \left(\frac{\partial C_\ell^{\phi\phi}}{\partial p_\alpha}\right)(\text{Cov}_{\ell\ell'}^R)^{-1}\left(\frac{\partial C_{\ell'}^{\phi\phi}}{\partial p_\beta}\right), \quad (20)$$

the Fisher matrix of a direct reconstruction of $C_\ell^{\phi\phi}$.

We will make the approximation that the covariance matrix $\text{Cov}_{\ell\ell'}^R$ of the reconstructed ϕ band powers is given by the Gaussian expression

$$\text{Cov}_{\ell\ell'}^R = \frac{2}{f_{\text{sky}}(2\ell+1)}(C_\ell^{\phi\phi} + N_\ell^{\phi\phi})^2\delta_{\ell\ell'}, \quad (21)$$

where $N_\ell^{\phi\phi}$ is the noise power spectrum of the reconstruction. We use as a baseline two cases: a hypothetical cosmic variance limited lens measurement where $N_\ell^{\phi\phi} = 0$, and the idealized reconstruction noise coming from the lens reconstruction from quadratic combinations of CMB fields. For details on how this reconstruction noise is calculated, see Ref. [31].

The Gaussian approximation (21) makes several approximations which we state explicitly. The power spectrum of the lens reconstruction contains an off-diagonal contribution from ϕ band powers [32] (this is the "N_1" bias found by Ref. [33]) which should be folded into the covariance $\text{Cov}_{\ell\ell'}^R$. It is also possible that there are contributions from higher-order terms in ϕ [34] (this is the "N_2" bias found by Ref. [35]); such contributions have been found to be small for temperature-based lens reconstruction, but this has not been checked for polarization. Finally, since the quadratic lens reconstruction is not a Gaussian field, its band power covariance may differ from the Gaussian expression (21). For temperature-based lens reconstruction, this issue has been studied in Ref. [35] and the Gaussian expression has been found to be a good

approximation (after slightly modifying the estimator along the lines of Ref. [36], see also Ref. [34] for alternate schemes), but the polarization case has not been studied. A complete treatment of these issues would be very interesting but is outside the scope of this paper; we will use the Gaussian approximation (21) as a first-order approximation to the exact Fisher matrix for lens reconstruction.

Note that the inverse of the Fisher matrix is an approximation for the covariance matrix of p_α

$$\text{Cov}_{\alpha\beta} = (\mathbf{F}^{-1})_{\alpha\beta} \quad (22)$$

for both the band power (P) and reconstruction (R) Fisher matrices.

B. Karhunen-Loève modes

While the p_α basis of lens power spectrum perturbations is complete, it is not ideally suited for assessing the information content or analysis of data. Measurements of the many individual parameters would be highly noisy (and correlated, in the case where the lensed CMB band powers D_i^{XY} are being used as the observable). In this section, we construct a more suitable basis whose eigenmodes are rank ordered in the relative information between CMB band powers and lens reconstruction. Moreover in the Fisher approximation, this basis provides a small set of relevant parameters whose errors are uncorrelated for both band power and direct measurements. As a complete basis, it can be used to study any cosmological parameter which affects the lensing potential.

To construct the eigenmodes, consider the KL transform:

$$\text{Cov}_{\alpha\beta}^P v_\beta^{(k)} = \lambda^{(k)}\text{Cov}_{\alpha\beta}^R v_\beta^{(k)}, \quad (23)$$

where $v_\beta^{(i)}$ and $\lambda^{(i)}$ are the KL eigenvectors and eigenvalues. We define the KL parameters m_k as linear combinations of the band perturbations or cosmological power spectrum deviations:

$$m_k = \sum_\alpha v_\alpha^{(k)}p_\alpha = \sum_\alpha v_\alpha^{(k)}\frac{1}{(\Delta\ell)_\alpha}\sum_\ell \delta\ln C_\ell^{\phi\phi}B_\alpha^{\phi,\ell}. \quad (24)$$

These KL modes have the property that their covariance, either measured from the lensed power spectra or from the reconstruction are diagonal and related by the KL eigenvalues. The eigenvectors are normalized such that all modes have unit variance for the direct reconstruction

$$\text{Cov}_{kk'}^R = \delta_{kk'} \quad (25)$$

and the KL construction then says that the eigenvalues are the relative variance from the CMB band powers

$$\text{Cov}_{kk'}^P = \lambda^{(k)}\delta_{kk'}. \quad (26)$$

The KL eigenvalues are therefore the ratio of the two covariances, and give a simple quantitative way to

determine which provides more information. If $\lambda^{(k)} < 1$, the corresponding KL mode m_k is better constrained by the power spectra than by the direct reconstruction.

C. CMB and lens cosmic variance

The KL construction allows a powerful test of physical self-consistency of the band power covariance. If we consider an idealized measurement in which both the lensed CMB and the lensing potential are cosmic variance limited (i.e., $N_\ell^{XY} = N_\ell^{\phi\phi} = 0$), then all KL eigenvalues must be ≥ 1, since there cannot be more information in the lensed CMB band powers than the reconstruction. We also consider in this section that the full sky is observed, i.e., $f_{\text{sky}} = 1$.

If we treat the lensed B mode as a Gaussian field [i.e., keep only the first term in the BB covariance (11)] then there are KL eigenvalues that strongly violate this physicality bound. For example, if we suppose that the BB power spectrum is measured to $\ell_{\text{max}} = 2000$, then we find $\lambda_{\text{min}} = 0.1$. This problem disappears when we include the full band power covariance: we find $\lambda_{\text{min}} = 1.4$, showing that our covariance model passes this consistency test. These results are in agreement with Refs. [12,29].

At $\ell_{\text{max}} = 3000$, we find that all the polarization-related non-Gaussian covariances must be included in order to satisfy the physicality bound $\lambda_{\text{min}} \gtrsim 1$. For example, let us suppose that only EE and BB power spectra are measured (including TT and TE would only strengthen the example). If we make the Gaussian approximation for $\text{Cov}^{EE,EE}$, but use non-Gaussian values for $\text{Cov}^{EE,BB}$ and $\text{Cov}^{BB,BB}$, then we find $\lambda_{\text{min}} = 0.9$ and fail the consistency test. Analogously, if we make the Gaussian approximation for $\text{Cov}^{EE,BB}$, but use non-Gaussian $\text{Cov}^{EE,EE}$ and $\text{Cov}^{BB,BB}$, then we find $\lambda_{\text{min}} = 0.8$ and fail. When we include the full non-Gaussian covariance model from Sec. II, then we do not find any violation of physicality, even when all band powers TT, TE, EE, BB are included. In that case, considering all the covariance as Gaussian leads to $\lambda_{\text{min}} = 0.07$. When the full non-Gaussian covariance from Sec. II is used, we have $\lambda_{\text{min}} = 1.09$ for the analytic covariance results, and $\lambda_{\text{min}} = 1.11$ when we use the covariance matrices computed from the simulations. We thus expect cosmological parameter errors to be modeled to better than a few percent for $\ell_{\text{max}} \lesssim 3000$. We quantify this expectation for parameter examples in Sec. IV C. Our model captures the essential of the non-Gaussian structure of the lensed power spectra covariance. Most terms in this covariance model have been neglected in previous studies.

D. Finite noise

While with a perfect reconstruction of the lensing potential power spectrum we cannot expect more information from the power spectra, considering a realistic

TABLE I. Instrumental specifications used in this paper. Sensitivities are given in μK arcmin.

Name	Frequency	Δ_T	Δ_P	θ_{FWHM}	f_{sky}	ℓ_{max}
Planck	100 GHz	81	115	9.5′	0.8	2000
	143 GHz	47	79	7.1′	0.8	2000
	217 GHz	71	122	4.7′	0.8	2000
Ground based		1.0	1.41	1′	0.016	3000
CMBPol		1.0	1.41	1′	0.8	3000

reconstruction with a finite noise could in principle lead to some modes which are better constrained by the power spectra than by reconstruction.

In Table I, we show some instrumental specifications that will be used throughout this paper. For Planck, we use the lowest three HFI frequencies with measured noise levels from Ref. [37], with maximum multiple $\ell_{\text{max}} = 2000$ and $f_{\text{sky}} = 0.8$.

We also consider a futuristic CMB polarization satellite (denoted by "CMBPol") with a low noise level ($\Delta_T = 1$ μK arcmin) and a resolution similar to the SPTPol experiment [38]. Finally, we consider a ground experiment with instrumental characteristics from CMBPol assuming a 650 deg^2 survey and Planck sensitivity on the remainder of the Planck region (i.e., $f_{\text{sky}} = 0.784$). We call this combination of Planck + ground-based experiment "Planck + G."

The instrumental noise power spectrum for a single channel is [39]:

$$N_\ell^{XX} = \left(\frac{\Delta_{XX}}{T_0}\right)^2 e^{\ell(\ell+1)\theta_{\text{FWHM}}^2/8\ln 2}, \qquad (27)$$

where $XX = TT$, EE, BB. For a multichannel experiment, the noise power spectrum is $N_\ell = (\sum_i N_{\ell(i)}^{-1})^{-1}$, where $N_{\ell(i)}$ is the noise power spectrum of the ith channel.

Note that even though CMBPol approaches the cosmic variance limit of the CMB, it does not reach the cosmic variance limit of lens reconstruction. The cosmic variance of the CMB fields themselves places an irreducible noise floor on even idealized reconstruction from quadratic estimators.

The KL eigenvalues are almost always larger than one, indicating that all the KL modes are better constrained by reconstruction than with the power spectra. The only exception is for CMBPol with a low cutoff at $\ell_{\text{max}} = 2000$. In that case $\lambda_{\text{min}} = 0.89$, indicating that one KL mode is slightly better constrained by lensed CMB power spectra than by lens reconstruction. This number merely reflects the fact that given the low noise and beam of the CMBPol experiment, applying a cutoff at $\ell_{\text{max}} = 2000$ degrades the ability of the lensing quadratic estimator to reconstruct the lensing potential.

All the other KL eigenvalues are greater than one and they rapidly become much larger after the third
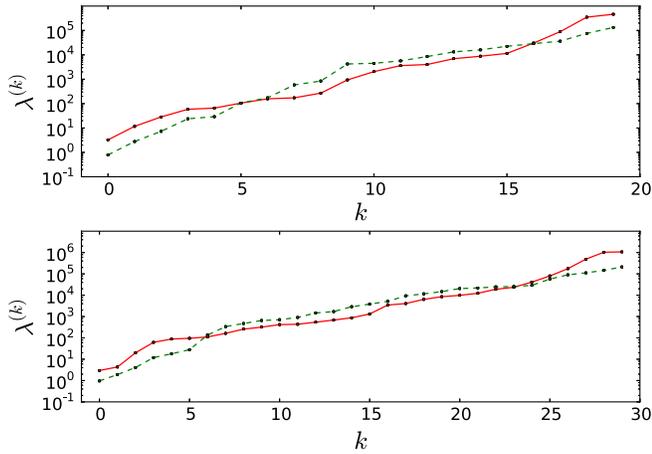
FIG. 6 (color online). KL eigenvalues for Planck (solid/red) and CMBPol (dashed/green). Top: $\ell_{\max} = 2000$. Bottom: $\ell_{\max} = 3000$.

mode (see Fig. 6), indicating that only one or two KL modes actually contribute to the lensed CMB power spectra, which is in agreement with Ref. [21].

IV. CONSTRAINTS ON COSMOLOGICAL PARAMETERS

Although the KL construction reveals extra information in lens reconstruction not available to lensed power spectra, accessing this information does not necessarily improve constraints on realistic cosmological parameters. Its impact depends on both how strongly and how uniquely cosmological parameter variations change the KL mode amplitudes corresponding to the new information.

Our purpose is not to give exhaustive forecasts on cosmological parameters for various experimental configurations. Rather, we wish to provide examples for when the extra KL information in reconstruction can and cannot make an impact. In Sec. IV A, we define and test a means of comparing the two in the presence of parameters that change the acoustic peaks of the unlensed CMB. In Sec. IV B, we compare the errors from the power spectra to the reconstruction and we assess the impact of the non-Gaussian covariance in Sec. IV C.

A. Additive lensing approach

The KL mode decomposition is complete and hence the errors on the mode amplitudes m_k can be used to construct the Fisher matrices $F_{cc'}^{\mathrm{KL},P}$, $F_{cc'}^{\mathrm{KL},R}$ corresponding to lensed power spectra and lens reconstruction, for any set of cosmological parameters c:

$$F_{cc'}^{\mathrm{KL},P} = \sum_k \frac{1}{\lambda^{(k)}} \frac{\partial m_k}{\partial c} \frac{\partial m_k}{\partial c'}, \quad F_{cc'}^{\mathrm{KL},R} = \sum_k \frac{\partial m_k}{\partial c} \frac{\partial m_k}{\partial c'}. \quad (28)$$

In other words, lensed CMB power spectrum constraints are downgraded (relative to lens reconstruction) by the KL

eigenvalues. In practice, there are only a few eigenvalues which are not $\gg 1$, and so lensed CMB power spectra are only sensitive to the first few eigenmodes.

The derivatives $(\partial m_k/\partial c)$ appearing above can be computed from Eq. (24):

$$\frac{\partial m_k}{\partial c} = \sum_\alpha v_\alpha^{(k)} \frac{1}{(\Delta\ell)_\alpha} \sum_\ell \frac{\partial \ln C_\ell^{\phi\phi}}{\partial c} B_\alpha^{\phi,\ell}. \quad (29)$$

Some values of these derivatives with respect to neutrino mass, dark energy equation of state, and curvature are presented in Fig. 7. They show a general decreasing trend but are not monotonically decreasing. For example, the neutrino mass derivative with $\ell_{\max} = 2000$ shows a second peak at the sixth KL mode (Fig. 7, left top panel).

The KL Fisher matrices are designed to only account for the information carried by CMB lensing and should be added to any other source of information. Indeed these matrices are highly degenerate if the parameters that control the unlensed CMB acoustic peaks are allowed to vary. Two options are conceivable depending on the objective. If one wants to compare the ultimate amount of information on the lensing parameters carried by CMB lensing through the band power measurements or through a lens reconstruction, then fixing the high-redshift parameters in the KL matrices is a possibility. In this case, we expect the KL treatment to be fully accurate within the Fisher approximation, but the resultant error estimates are not meaningful unless other sources of information fix those parameters.

The second approach is to add other sources of information to the Fisher matrix. The current leading source of information on these parameters is of course the acoustic peaks themselves. The bulk of this information comes from the unlensed CMB spectra. To the extent that the lensing simply adds to the information in the unlensed CMB we can approximate the total Fisher matrix as the sum

$$F^{\mathrm{KL},PU} = F^{\mathrm{KL},P} + F^U, \qquad F^{\mathrm{KL},RU} = F^{\mathrm{KL},R} + F^U, \quad (30)$$

where F^U is the Fisher matrix constructed out of the unlensed CMB fields with a Gaussian covariance. We call this the "additive lensing" approximation. For lensing parameters where lensing can actually destroy information in the power spectrum, such as Ω_K [21] and m_ν at sufficiently large values that the neutrinos are nonrelativistic at recombination, this treatment is approximate. On the other hand it is an approximation that affects the lensing reconstruction and power spectrum information alike.

For the power spectrum information, there is a direct check of this approximation since we can construct the Fisher matrix from the lensed power spectra and the power spectrum covariance

$$F_{cc'}^{\mathrm{dir},P} = \sum_{IJ} \left(\frac{\partial D_I}{\partial c}\right) (\mathrm{Cov}_{IJ}^{D,D})^{-1} \left(\frac{\partial D_J}{\partial c'}\right). \quad (31)$$
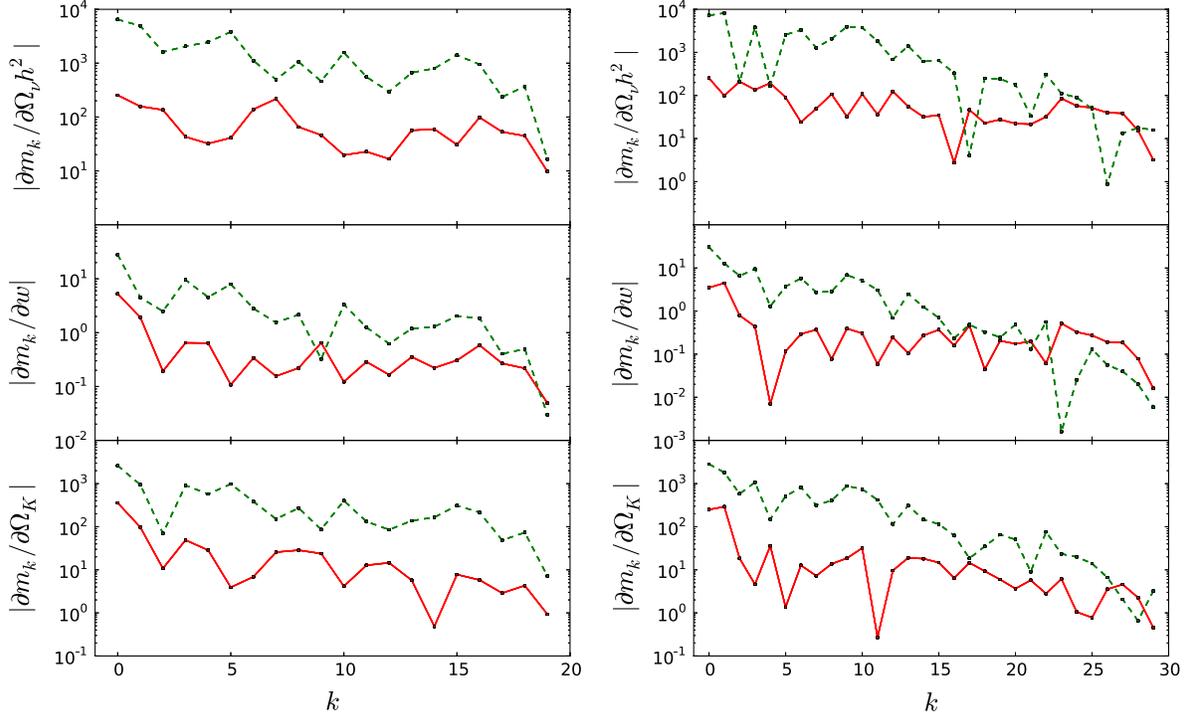
FIG. 7 (color online).   Derivatives of the KL modes m_k with respect to $\Omega_\nu h^2$ (top), w (middle), and Ω_K (bottom) with $l_{max} = 2000$ (left column) and $l_{max} = 3000$ (right column), for Planck (solid/red) and CMBPol (dashed/green).

For the reconstruction, a direct check of the additive lensing approximation would require understanding the covariance between reconstruction and power spectrum statistics, as well as more subtle effects such as the N_1 bias mentioned previously [40].

As an aside, note that for numerical stability when computing the power spectrum Fisher matrices it is important to pick a parameter set c where the angular diameter distance degeneracy is manifest. Hence in practice derivatives with respect to cosmological parameters are computed by adjusting the Hubble parameter h so that the acoustic scale is fixed when varying the values of other parameters. Our parameter basis is then composed of three lensing parameters ($\sum m_\nu$, w, and Ω_K) and six high-redshift parameters which control the unlensed CMB: $\{\Omega_c h^2, \Omega_b h^2, n_s, \tau, A_s e^{-2\tau}, \theta_S\}$, where θ_S is the angle subtended by the sound horizon at recombination. These six high-redshift parameters are marginalized in all parameter constraints presented in this paper.

We begin by testing the accuracy of the additive lensing approximation in the power spectrum case, where we can simply compare the Fisher matrix $F^{KL,PU}$ obtained in the additive lensing approximation [Eq. (30)] to the exact Fisher matrix $F^{dir,P}$ [Eq. (31)]. As can be seen in Fig. 8, which presents the ratio of the errors computed by the two different techniques for a single additional lens parameter, the two approaches are not strictly equivalent. As expected, this is especially true for Ω_K where the errors from the direct lensed Fisher matrix are typically 5% larger than

those predicted by our KL formalism and can approach 20% at high noise. For w, the difference in the errors is constant at about 3% over the range of noise level considered. Finally, for $\sum m_\nu$ and the high fiducial value of 0.58 eV, the agreement depends on the noise level. For very high levels of noise, most of the information comes from the first few peaks of the unlensed CMB and that information can be reduced by lensing. For very low levels
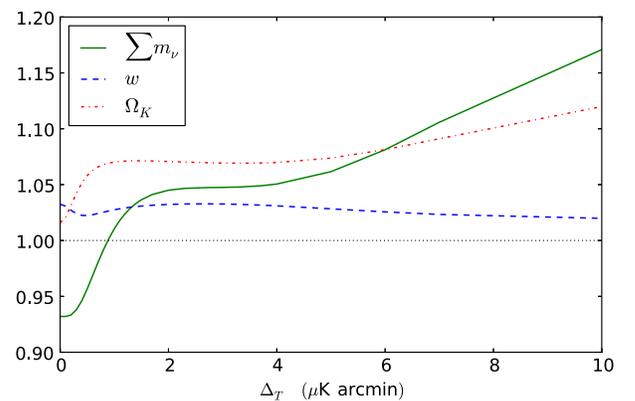
FIG. 8 (color online).   Ratio of statistical errors computed using the additive lensing approximation (i.e., $F^{KL,PU}$) and the exact Fisher matrix (i.e., $F^{dir,P}$) for individual lensing parameters, as a function of noise level for a $\theta_{FWHM} = 1'$, $\ell_{max} = 3000$ experiment. The error on each lensing parameter is computed with the other two lensing parameters fixed and high-redshift parameters marginalized.

of noise, the lensing information saturates to its sample variance level, while the unlensed CMB would have in principle retained information far out into the exponentially damped tail. In the intermediate noise regime of interest to future CMB polarization experiments, the additive lensing approximation is accurate. Furthermore, we have explicitly verified that as the fiducial value for $\sum m_\nu$ is lowered, the discrepancy rapidly goes away.

The same general trends apply to cases of multiple lensing parameters. As an example, we show in Fig. 9 (top panel) the constraints in the ($\sum m_\nu$)-w plane (Ω_K being fixed) for the Planck + G and CMBPol experiments. The ellipses from the two approaches are in very good agreement, thus validating the additive approach in the case where curvature is fixed.
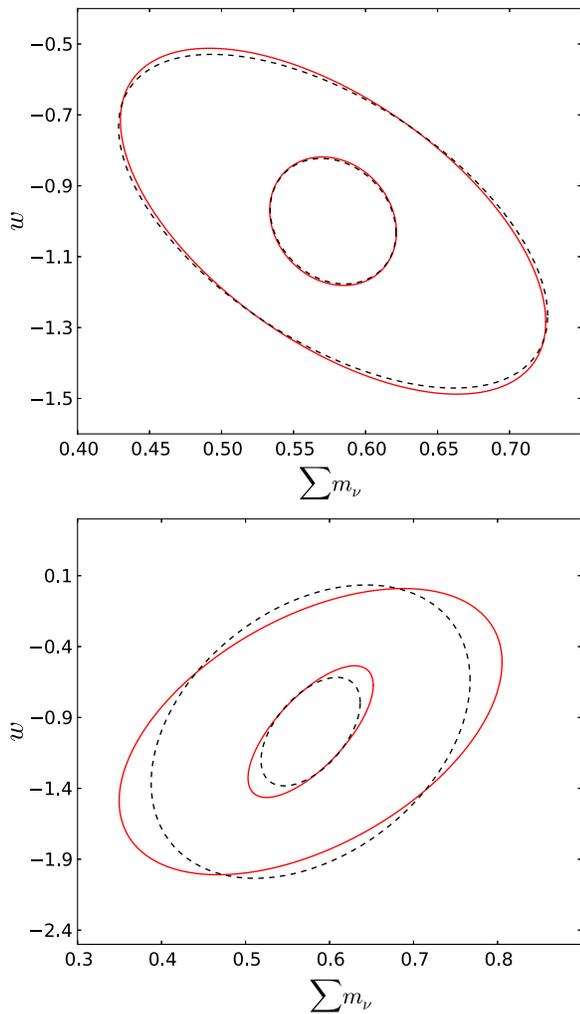
FIG. 9 (color online). Sixty-eight percent confidence limit (CL) ellipses in the ($\sum m_\nu$)-w plane for the Planck + G (outer ellipses) and CMBPol (inner ellipses) experiments. Errors using the additive lensing approximation ($F^{\mathrm{KL},PU}$) are shown in dashed/black, and errors using the exact Fisher matrix ($F^{\mathrm{dir},P}$) are shown in solid/red. Top: Ω_K is fixed. Bottom: Ω_K is marginalized.

In the case where curvature is allowed to vary (bottom panel), parameters become highly degenerate in the lensed power spectrum effects and so the impact of unlensed information becomes larger. For the CMBPol case the errors in $\sigma(m_\nu)$ with w and curvature marginalized are larger by a factor of 1.26 and for the Planck + G experiment they are larger by 1.20 when comparing the exact to the additive approach. When making comparisons between reconstruction and power spectrum information in such degenerate cases with curvature, one must bear in mind these curvature induced problems [41].

In summary, for the interesting cases where lensing provides most of the information on the lensing parameters, the additive lensing approximation is accurate in the power spectrum case (i.e., the Fisher matrices $F^{\mathrm{KL},PU}$ and $F^{\mathrm{dir},P}$ agree). The additive lensing approximation is very convenient for comparing the cosmological information from lensed CMB power spectra and lens reconstruction. Since the Fisher matrix is separated into a sum of unlensed and lensed contributions, we can simply compare the Fisher matrices $F^{\mathrm{KL},PU}$ and $F^{\mathrm{KL},RU}$ defined in Eq. (30). This provides a metric for relative comparison of power spectrum and reconstruction lensing information.

B. Power spectra vs reconstruction

Given the results in the last section, we can compare cosmological parameter constraints from lens reconstruction and lensed CMB power spectra. Moreover, using the KL eigenmode formalism, we can explicitly verify how many KL modes actually carry the cosmological information.

As a general statement, we find that reconstruction always carries more information than the lensed power spectra, regardless of the parameter considered. As the KL modes are rank-ordered in terms of highest relative information content in the power spectra, we can choose to truncate the summation defining the KL Fisher matrices [Eq. (28)] to only use the information from the first few KL modes. Those cumulative errors are presented in Fig. 10 (upper) for cases where there is only a single additional lensing parameter. This case is the easiest to understand since the power spectrum information will be dominated by the first eigenmode.

For CMBPol, the first KL eigenvalue is close to 1 and so the errors for any individual lensing parameter are comparable. The power spectrum information saturates at 2–3 eigenmodes as expected. These are modes for which the extra information in the reconstruction becomes manifest, but for the three chosen lensing parameters the total impact is small for Ω_K and w, given the dominance of the first mode in the derivatives in Fig. 7. For the neutrinos there is a somewhat larger effect corresponding to large derivatives in both of the first two modes. Note also that for reconstruction the eigenmodes are not rank-ordered so some of the higher modes can contribute more information than the lower modes. For neutrinos, the cumulative reduction of
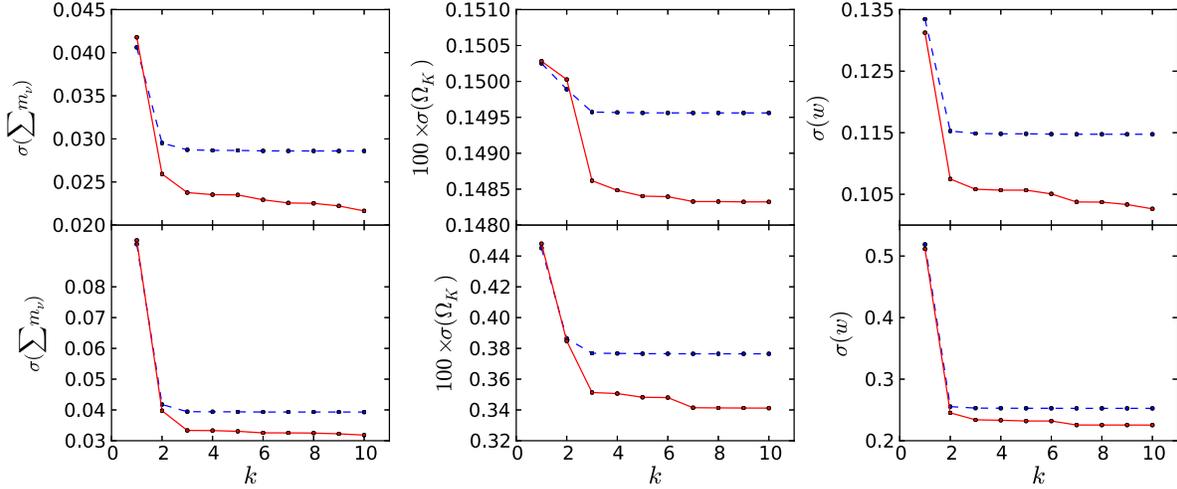
FIG. 10 (color online). Statistical errors on $\sum m_\nu$ (left), Ω_K (middle), and w (right) from lens reconstruction (solid/red) and lensed CMB power spectra (dashed/blue), using the first k KL eigenmodes (where $1 \leq k \leq 10$), for CMBPol specs with $\ell_{\max} = 3000$. As expected, KL eigenmodes with $k \geq 3$ do not contribute to the power spectrum constraints, but can contribute slightly in the lens reconstruction case. Statistical errors were computed using the "additive lensing" approximation and the Fisher matrices $F^{\mathrm{KL},PU}$ and $F^{\mathrm{KL},RU}$, as described in Sec. IVA. Top row: only one lensing parameter is varied and the other two are fixed. Bottom row: all three are varied with the two not shown marginalized.

errors from the reconstruction (relative to the power spectrum constraint) reaches 0.7–0.8.

When more than one lensing parameter is included, resulting degeneracies can make the information in reconstruction more important. However the small derivatives in Fig. 7 still limit the practical relevance of this information, in that other sources like the unlensed CMB and more importantly other cosmological probes quickly dominate the net information.

In Fig. 11, we show a two-dimensional example: comparison of power spectrum and lens reconstruction constraints in the $(\sum m_\nu)$-w plane with Ω_K fixed, for Planck and CMBPol. Let us interpret this figure in light of our KL eigenmode construction. For Planck (upper panel), there is one (roughly vertical) direction which is constrained by CMB lensing, and the lens reconstruction constraint is stronger than the lensed power spectrum constraint. There is another (roughly horizontal) direction which is constrained by lens reconstruction, but very weakly constrained by *lensing* information in the power spectrum (it is constrained by the unlensed power spectrum). This is consistent with the KL eigenvalues for Planck shown in Fig. 6: there is one KL eigenvalue which is a little larger than 1, and the second KL eigenvalue is $\gg 1$. For CMBPol (bottom panel of Fig. 11), there is one direction where the lensed power spectrum and lens reconstruction constraints are nearly exactly equal, and another direction where lens reconstruction is somewhat better. This is consistent with the KL eigenvalues in Fig. 6: the lowest KL eigenvalue is almost exactly equal to 1, and the second KL eigenvalue is ~ 2.

Similarly, although the KL analysis would imply that with 3 lensing parameters there should be substantially better lensing reconstruction constraints, for the chosen

parameters and their fiducial values the unlensed CMB information rapidly dominates. In Fig. 10 (lower), we show the impact on the parameter errors of marginalizing the other two lensing parameters. In this case, all three types of lensing parameters show 10% or greater cumulative improvements from the reconstruction due to the higher modes breaking degeneracies, but they are still of the same order of magnitude as those of the power spectra. Further relative improvements here are limited by the unlensed CMB information which also weakly breaks these degeneracies in the additive approach. Note that we are somewhat underestimating the impact of the extra reconstruction information when considering CMB-only sources of information, since this ability to break degeneracies in the unlensed CMB is degraded by lensing. Nonetheless the main point that in practice the extra information accessible to lensing reconstruction with CMBPol is mainly orthogonal to realistic cosmological parameters remains.

C. Impact of non-Gaussian covariance

We conclude our analysis by investigating the impact of the non-Gaussian covariance of the lensed power spectra on the final errors on parameters. Since this does not involve reconstruction information, we work here with the direct lensed power spectra Fisher matrix $F^{\mathrm{dir},P}$, rather than using the "additive lensing" approximation from Sec. IVA.

First note that if one considers the amplitude of the fiducial lensing spectrum $C_\ell^{\phi\phi} = A_{\mathrm{lens}} C_\ell^{\phi\phi}|_{\mathrm{fid}}$ as the independent lensing parameter as often done in the current literature [8,9], then non-Gaussian modeling is required
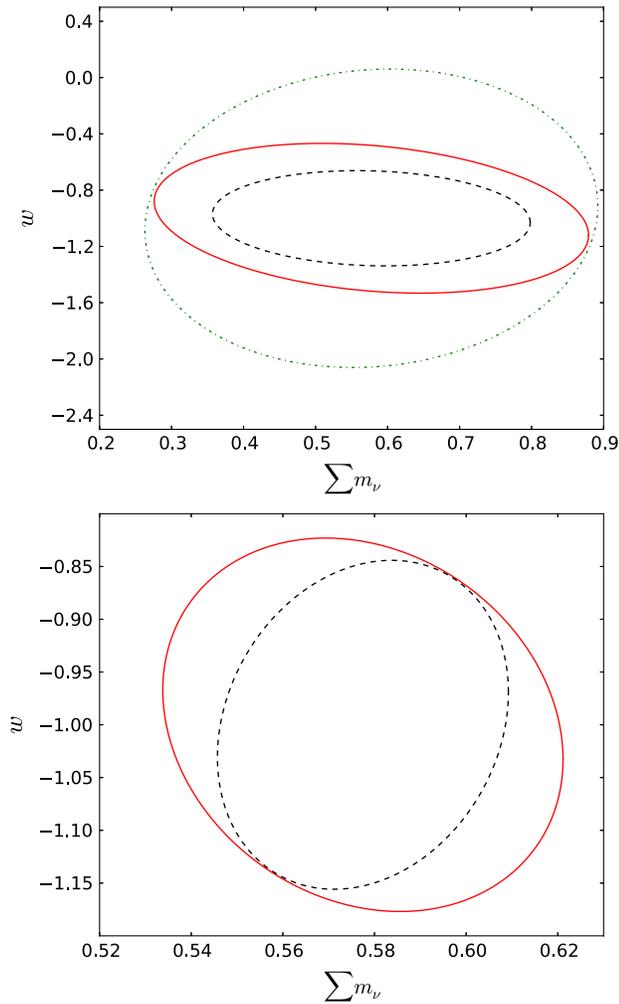
FIG. 11 (color online). Comparison of 68% CL ellipses in the $(\sum m_\nu)$-w plane obtained from lens reconstruction (black/dashed) and lensed CMB power spectra (red/solid). Statistical errors are computed using the additive lensing approximation (i.e., Fisher matrices $F^{\mathrm{KL},RU}$ and $F^{\mathrm{KL},PU}$) and fixed Ω_K, for Planck (top panel) and CMBPol (bottom panel, $\ell_{\max} = 3000$). The outer ellipse in the top panel is *unlensed* CMB constraint (not shown in the bottom panel since the unlensed constraint is much weaker than the lensed constraint).

FIG. 12 (color online). Sixty-eight percent CL ellipses in the $(\sum m_\nu)$-w plane, computed using the exact Fisher matrix $F^{\mathrm{dir},P}$ with fixed Ω_K, for the Planck + G (top) and CMBPol (bottom, $\ell_{\max} = 3000$) experiments. Dash-dotted magenta lines are computed with the full Gaussian covariance matrix, and solid red lines with the full non-Gaussian covariance from the semianalytical model. Dashed black lines are computed using an intermediate covariance matrix which includes the non-Gaussian BB-BB covariance, but Gaussian covariance for all combinations of T and E.

for any experiment that gains information from polarization. This follows from our KL treatment where the information on the amplitude comes almost exclusively from the first mode. For example for CMBPol and $\ell_{\max} = 3000$, $\sigma(A_{\mathrm{lens}}) = 0.0011$ for Gaussian covariance and $\sigma(A_{\mathrm{lens}}) = 0.002395$ for the non-Gaussian covariance from the simulations. Our analytic model captures this degradation to 2.8% yielding $\sigma(A_{\mathrm{lens}}) = 0.002329$.

If on the other hand one takes the lensing parameters as fundamental cosmological parameters, the impact of non-Gaussianity is hidden by marginalizing their impact on $C_\ell^{\phi\phi}$. In the previous studies where only the dominant BB-BB covariance was considered [21] the impact of non-Gaussianity on lensing parameters was small once

the power spectra amplitude A_s and the dark matter density $\Omega_c h^2$ were marginalized for $\ell_{\max} < 2000$. This simplification has been employed in the subsequent literature to study parameter forecasts in a wider range of scenarios [42].

The analytic model allows us to separate out the impact of the new EE and TE covariance terms. In Fig. 12, we show the net impact on the w-$\sum m_\nu$ errors of including the non-Gaussian terms on the Planck + G (top) and CMBPol (bottom) experiments, with all the high-redshift parameters marginalized but Ω_K fixed. For the Planck + G experiment the overall impact is small as one would expect from just adding BB lensing information to Planck. For the CMBPol experiment, there is a more substantial effect. Interestingly

this degradation is almost entirely due to the new EE and TE terms and can be attributed to the use of lensing information in these spectra to break degeneracies between lensing parameters and high-redshift parameters.

These new terms can have an impact even if there is only one additional lensing parameter. For the CMBPol experiment if $\sum m_\nu$ and Ω_K are fixed, the error on w with the full non-Gaussian covariance is $\sigma(w) = 0.118$. However, if only the non-Gaussian BB-BB covariance is used, we have $\sigma(w) = 0.095$, a 24% difference. We conclude that if in the future lensing information out to $\ell_{\max} = 3000$ from the polarization fields becomes available and dominates parameter errors, then all of the covariance terms that involve polarization should be modeled for full accuracy.

V. CONCLUSIONS

We have constructed a semianalytic model of the covariance matrix of the lensed power spectra of CMB temperature and polarization anisotropies. This model is able to reproduce the structure found in simulations of CMB lensing for the non-Gaussian terms in this covariance. More specifically, we have shown the existence and importance of second-order terms in the lensing potential that were unaccounted for in previous studies [21–23]. Our model captures these effects and enables an efficient quantification of cosmological parameter errors that matches simulations to better than $\sim 3\%$ for $\ell_{\max} \leq 3000$ even in cases where the non-Gaussianity causes an order unity degradation in the errors.

Using an parameter independent approach based on the decomposition of the information carried by CMB lensing in terms of Karhunen-Loève eigenmodes, we have exhibited some cases where neglecting some of these second-order terms leads to physical inconsistencies. These inconsistencies are removed once the covariance from our model is used.

We then applied the KL eigenmode technique to compare the cosmological information that can be extracted either from measurements of the lensed power spectra or by reconstruction of the lensing potential using quadratic estimators. Although the non-Gaussian covariance of the lensed spectra has no significant impact on parameter errors for Planck, we found that it is non-negligible for forthcoming CMB experiments which will probe polarization at the arcminute scale.

If the full non-Gaussian covariance is used then there is always more information, in principle, in the reconstruction than in the lensed power spectra. In practice, the removal of various biases in the reconstruction and higher-order terms in the reconstruction covariance matrix may degrade the final errors on parameters. Furthermore, this extra information is mainly in the detailed shape of the power spectrum of the lenses. Typical cosmological parameters do not access this information as they mainly change the amplitude of the spectrum.

The work presented here is one element in a joint and optimal likelihood analysis of CMB lensing. Our covariance model provides a computationally efficient means of calculating the covariance matrix of lensed CMB power spectra as a function of underlying cosmological or lens parameters. In the future, a full joint analysis will require more accurate techniques for a similar characterization of the reconstruction covariance as well as the covariance between power spectra and reconstruction observables.

APPENDIX: DERIVATIVE APPROXIMATION FOR NON-GAUSSIAN COVARIANCE

The covariance of BB with EE, TT, or TE [see Eq. (13)] involves computing derivatives of lensed CMB power spectra with respect to unlensed spectra

$$\sum_\ell \left(\frac{\partial C_{\ell_1}^{BB}}{\partial C_\ell^{\tilde{E}\tilde{E}}} \text{Cov}_{\ell\ell}^{\tilde{E}\tilde{E},\tilde{X}\tilde{Y}} \frac{\partial C_{\ell_2}^{XY}}{\partial C_\ell^{\tilde{X}\tilde{Y}}} \right). \tag{A1}$$

First note that $\partial C_{\ell_1}^{BB}/\partial C_\ell^{\tilde{E}\tilde{E}}$ is a slowly varying function of both ℓ_1 and ℓ given the broad kernel that transfers power between the $\tilde{E}\tilde{E}$ and BB. Thus the derivative can be well approximated by the average response to an unlensed band perturbation of width $\Delta L_\alpha = 10$ for $\ell \in$ band

$$\frac{\partial C_{\ell_1}^{BB}}{\partial C_\ell^{\tilde{E}\tilde{E}}} \approx \frac{\partial C_{\ell_1}^{BB}}{\partial p_\alpha^{\tilde{E}\tilde{E}}} \frac{1}{\Delta L_\alpha} \frac{1}{C_\ell^{\tilde{E}\tilde{E}}}. \tag{A2}$$

On the other hand $\partial C_{\ell_2}^{XY}/\partial C_\ell^{\tilde{X}\tilde{Y}}$ cannot in general be approximated by a band response as it will have both a smooth piece from lensing and a $\delta_{\ell_2,\ell}$ term from the unlensed CMB. However, to calculate the covariance it suffices to note that both the BB derivative and the Cov term are slowly varying on the ΔL_α scale. Thus the sum over $\ell \in B_\alpha$ means that we can replace the true derivative with the band average response again:

$$\left\langle \frac{\partial C_{\ell_2}^{XY}}{\partial C_\ell^{\tilde{X}\tilde{Y}}} \right\rangle_{\Delta L_\alpha} = \frac{\partial C_{\ell_2}^{XY}}{\partial p_\alpha^{\tilde{X}\tilde{Y}}} \frac{1}{\Delta L_\alpha} \frac{1}{C_\ell^{\tilde{X}\tilde{Y}}}. \qquad \text{(A3)}$$

With this replacement

$$\sum_\ell \left(\frac{\partial C_{\ell_1}^{BB}}{\partial C_\ell^{\tilde{E}\tilde{E}}} \text{Cov}_{\ell\ell}^{\tilde{E}\tilde{E},\tilde{X}\tilde{Y}} \frac{\partial C_{\ell_2}^{XY}}{\partial C_\ell^{\tilde{X}\tilde{Y}}} \right)$$

$$\approx \sum_\alpha \left[\frac{\partial C_{\ell_1}^{BB}}{\partial p_\alpha^{\tilde{E}\tilde{E}}} \frac{\partial C_{\ell_2}^{XY}}{\partial p_\alpha^{\tilde{X}\tilde{Y}}} \frac{1}{(\Delta L_\alpha)^2} \sum_{\ell \in B_\alpha} \frac{\text{Cov}_{\ell\ell}^{\tilde{E}\tilde{E},\tilde{X}\tilde{Y}}}{C_\ell^{\tilde{E}\tilde{E}} C_\ell^{\tilde{X}\tilde{Y}}} \right]. \qquad \text{(A4)}$$

Note that while not necessary here, the derivatives can alternately be calculated more exactly by perturbing single ℓ's on a sparse grid in the unlensed ℓ. As a function of the unlensed ℓ the derivatives can be separated as

$$\frac{\partial C_{\ell_1}^{XY}}{\partial C_\ell^{\tilde{X}\tilde{Y}}} = A_\ell \delta_{\ell\ell_1} + B_{\ell\ell_1} \qquad \text{(A5)}$$

into two slowly varying pieces A_ℓ and $B_{\ell\ell_1}$.

[1] A. Blanchard and J. Schneider, Astron. Astrophys. **184**, 1 (1987).
[2] F. Bernardeau, Astron. Astrophys. **338**, 767 (1998).
[3] M. Zaldarriaga and U. Seljak, Phys. Rev. D **59**, 123507 (1999).
[4] A. Lewis and A. Challinor, Phys. Rep. **429**, 1 (2006).
[5] K. M. Smith, O. Zahn, and O. Doré, Phys. Rev. D **76**, 043510 (2007).
[6] C. M. Hirata, S. Ho, N. Padmanabhan, U. Seljak, and N. A. Bahcall, Phys. Rev. D **78**, 043520 (2008).
[7] S. Das, B. D. Sherwin, P. Aguirre, J. W. Appel, J. R. Bond *et al.*, Phys. Rev. Lett. **107**, 021301 (2011).
[8] B. D. Sherwin, J. Dunkley, S. Das, J. W. Appel, J. Bond *et al.*, Phys. Rev. Lett. **107**, 021302 (2011).
[9] A. van Engelen, R. Keisler, O. Zahn, K. Aird, B. Benson *et al.*, Astrophys. J. **756**, 142 (2012).
[10] R. B. Metcalf and J. Silk, Astrophys. J. Lett. **492**, L1 (1998).
[11] R. Stompor and G. Efstathiou, Mon. Not. R. Astron. Soc. **302**, 735 (1999).
[12] W. Hu, Phys. Rev. D **65**, 023003 (2001).
[13] M. Kaplinghat, L. Knox, and Y.-S. Song, Phys. Rev. Lett. **91**, 241301 (2003).
[14] V. Acquaviva and C. Baccigalupi, Phys. Rev. D **74**, 103510 (2006).
[15] W. Hu, Phys. Rev. D **62**, 043007 (2000).
[16] K. Benabed, F. Bernardeau, and L. van Waerbeke, Phys. Rev. D **63**, 043501 (2001).
[17] J. Guzik, U. Seljak, and M. Zaldarriaga, Phys. Rev. D **62**, 043517 (2000).
[18] W. Hu, Astrophys. J. **557**, L79 (2001).
[19] W. Hu and T. Okamoto, Astrophys. J. **574**, 566 (2002).
[20] C. M. Hirata and U. Seljak, Phys. Rev. D **68**, 083002 (2003).
[21] K. M. Smith, W. Hu, and M. Kaplinghat, Phys. Rev. D **74**, 123002 (2006).
[22] S. Smith, A. Challinor, and G. Rocha, Phys. Rev. D **73**, 023517 (2006).

[23] C. Li, T. L. Smith, and A. Cooray, Phys. Rev. D **75**, 083501 (2007).
[24] M. D. Niemack *et al.*, Proc. SPIE Int. Soc. Opt. Eng. **7741**, 77411S (2010).
[25] B. Keating *et al.*, arXiv:1110.2101.
[26] A. Lewis, A. Challinor, and A. Lasenby, Astrophys. J. **538**, 473 (2000).
[27] K. M. Górski, E. Hivon, A. J. Banday, B. D. Wandelt, F. K. Hansen, M. Reinecke, and M. Bartelmann, Astrophys. J. **622**, 759 (2005).
[28] A. Lewis, Phys. Rev. D **71**, 083008 (2005).
[29] K. M. Smith, W. Hu, and M. Kaplinghat, Phys. Rev. D **70**, 043002 (2004).
[30] A. Challinor and A. Lewis, Phys. Rev. D **71**, 103010 (2005).
[31] T. Okamoto and W. Hu, Phys. Rev. D **67**, 083002 (2003).
[32] W. Hu, Phys. Rev. D **64**, 083005 (2001).
[33] M. Kesden, A. Cooray, and M. Kamionkowski, Phys. Rev. D **67**, 123507 (2003).
[34] W. Hu, S. DeDeo, and C. Vale, New J. Phys. **9**, 441 (2007).
[35] D. Hanson, A. Challinor, G. Efstathiou, and P. Bielewicz, Phys. Rev. D **83**, 043005 (2011).
[36] C. Dvorkin and K. M. Smith, Phys. Rev. D **79**, 043003 (2009).
[37] Planck HFI Core Team, Astron. Astrophys. **536**, A6 (2011).
[38] J. J. McMahon, K. A. Aird, B. A. Benson, L. E. Bleem, J. Britton *et al.*, in *The Thirteenth International Workshop on Low Temperature Detectors—LTD13*, American Institute of Physics Conference Series Vol. 1185, edited by B. Young, B. Cabrera, and A. Miller (AIP, New York, 2009), p. 511.
[39] L. Knox, Phys. Rev. D **52**, 4307 (1995).
[40] O. Zahn, R. de Putter, S. Das, and A. Yadav (unpublished).
[41] C. Howlett, A. Lewis, A. Hall, and A. Challinor, J. Cosmol. Astropart. Phys. 4 (2012) 027.
[42] R. de Putter, O. Zahn, and E. V. Linder, Phys. Rev. D **79**, 065033 (2009).